VI. Materials

ENGINEERING MECHANICS DIVISION

A. Carbon and Graphite, *D. B Fischbach*

1. Tensile Deformation Dimension Changes

Although brittle at ordinary temperatures, carbons and graphites exhibit considerable plasticity at high temperatures. An investigation is being made of the mechanisms of plastic deformation which are responsible for this high-temperature plasticity. Currently, attention is being directed to the deformation behavior of pyrolytic and vitreous carbons. Recent precise data on the gage-section dimension changes which accompany high-temperature tensile deformation parallel to the substrate in pyrolytic carbon have provided some significant clues to the nature of the active deformation processes.

It had been found that the tensile deformation of as-deposited pyrolytic carbon stressed parallel to the substrate occurs in two stages[1] (SPS 37-33, Vol. IV, pp. 75–81). Stage I is characterized by straightening of the initially wrinkled layer planes, and is accompanied by crystallite growth and the development of layer-plane stacking order (graphitization). At the end of stage I, after about 10% elongation, the sample gage section is well graphitized and highly oriented with the layer planes aligned closely parallel to the stress axis. Stage II deformation occurs in this highly oriented graphite. Earlier results showed that deformation occurs at approximately constant volume to at least 20% elongation. During stage I the width of the gage section (parallel to substrate) increased slightly, while the thickness (perpendicularly to the substrate) decreased rapidly, consistent with layer straightening. During stage II, the width and thickness appeared to decrease at approximately the same rate as a function of elongation[1] (Ref. 1).

More precise measurements have now confirmed these early results and revealed some significant details which were not apparent earlier. The better quality of the new data resulted from the use of ink-line fiducial marks and other improved techniques reported earlier (SPS 37-43, Vol. IV, pp. 121–125). The reduction in cross-sectional area as a function of uniform gage elongation is shown in Fig. 1. The solid-line curve was calculated on the assumption of constant volume. The data for pyrolytic carbon (circles) show that during stage I the volume of this material decreases (densification). During stage II the volume remains constant, about 2% less than the initial volume. This observed volume decrease is accounted for

[1]Fischbach, D. B., and Kotlensky, W. V., "On the Mechanism of High Temperature Plastic Deformation in Pyrolytic Carbons," *Electrochemical Technology*, to be published.

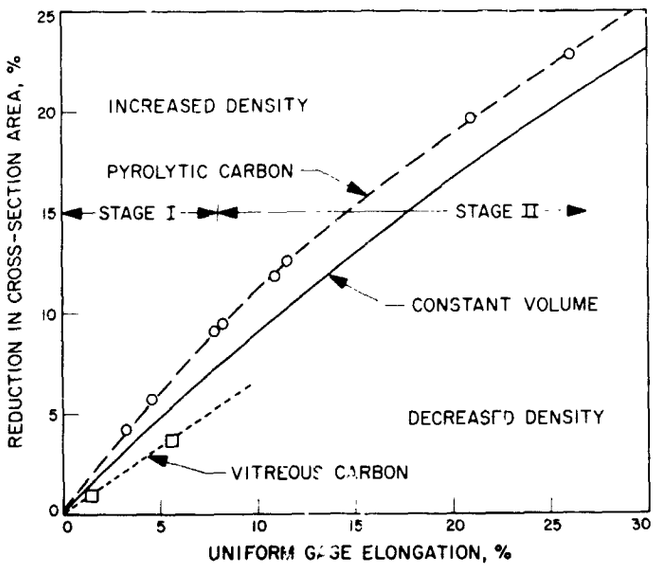

Fig. 1. Reduction in area as a function of tensile elongation for pyrolytic and vitreous carbons at 2500–2900°C

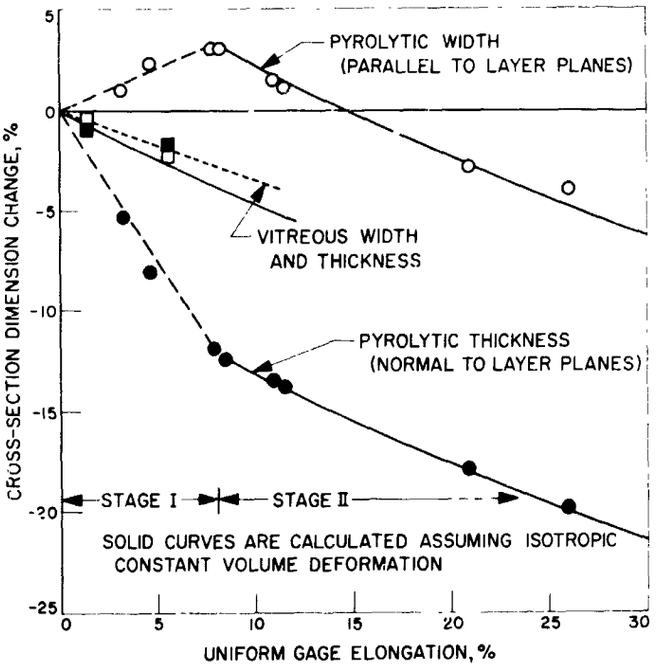

Fig. 2. Change in cross-section dimensions as a function of tensile elongation for pyrolytic and vitreous carbons at 2500–2900°C

by the 2% decrease in interlayer spacing, measured by x-ray diffraction, which accompanies graphitization. Initial results on vitreous carbon (squares) show that some volume increase accompanies tensile deformation in this material.

The changes in gage-section width and thickness with elongation are shown in Fig. 2. Stage I is completed at 8% elongation with a width increase of about 3.2% and a thickness decrease of 12% in this particular carbon. One-sixth of the thickness decrease (2%) may be attributed to graphitization, while the rest of the change in thickness and all of the width increase must be attributed to layer straightening. The solid lines in the stage II region were calculated on the assumption of isotropic (width and thickness decrease at same rate) constant volume deformation beginning at 8.0% elongation. Within the precision of the data, the results for pyrolytic carbon agree very well with the expected behavior of an isotropic material! The results on vitreous carbon show that it also deforms isotropically, but not at constant volume, consistent with the reduction in area data. This behavior is expected for vitreous carbon, which has a macroscopically isotropic porous structure. Isotropic deformation in pyrolytic carbon is quite unexpected because the structure is highly anisotropic. The changes in gage-section length and width occur parallel to the layer planes; changes in thickness occur perpendicular to the layer planes. Most properties of graphite differ greatly parallel and perpendicular to the layer planes.

The observed isotropy of dimension changes in pyrolytic carbon stage II deformation has significant implications for the deformation mechanisms and associated processes such as diffusion. If deformation occurs primarily by a dislocation mechanism, then slip must occur with equal ease on prism- and pyramid-type planes. If Nabarro-Herring diffusion mass transport is the dominant deformation mechanism, as suggested by current studies on the stress dependence of the creep rate (SPS 37-43, Vol. IV, pp. 121–125) then diffusion transport of atoms from the layer plane face and edge sides to the edge ends of the crystallites must occur at the same rate. From this it may be inferred that there is little difference in diffusion rate parallel and perpendicular to the layer planes. More information on deformation and diffusion mechanisms in graphite is required to determine the true significance of these results.

2. Some Bending and Kinking Deformation Effects

It is well known that graphite will deform by kinking and twinning under compression parallel to the layer planes. In a twin, the layer planes bend sharply through a crystallographically prescribed angle along a crystallographically prescribed direction. A kink, as used here, is similar but the angle and line of bend are not crystallographically determined. More gradual bending is also

observed. Kink bands and bending are easily visible in polarized light micrographs of sections normal to the layer planes because of the sharp change in layer-plane orientation in the kink or bend. In the course of an investigation of the mechanisms of tensile deformation in pyrolytic carbon parallel to the substrate, several interesting varieties of kinking and bending deformation have been observed. All are incidental to the gage-section tensile deformation.

Frequently, the layer-plane faces of highly elongated ($\geq$ 10%) tensile specimens have bent-up ridges along the edges, especially in the throat regions. Fig. 3a shows a polarized light micrograph of a transverse cross section of the gage region of a deformed sample. (The location and orientation in the specimens of the micrographs in Figs. 3–6 are shown in Fig. 7.) The tensile stress was normal to the plane of the figure. The layer plane orientation is parallel to the cleavage and delamination cracks (the sample cleaved into two pieces during preparation). Throughout most of the cross section the layer planes are horizontal, but in wedge-shaped regions in the corners the planes are bent 28–47 deg away from the horizontal (the lower left corner is dark and cannot be distinguished). This peculiar phenomenon has been traced to adherent deposits of evaporated carbon from the graphite heater which condense on the specimen edges, especially near the grips (Fig. 3b). Deposits are not usually observed on the specimen faces; evidently the evaporated carbon does not adhere to layer-plane surfaces. X-ray diffraction showed that these deposits were well graphitized but randomly oriented. The thermal expansion coefficient of the deposited carbon would be expected to be $\leq 4 \times 10^{-6}$/°C; the expansion coefficient of the highly oriented pyrolytic gage section, perpendicular to the layer planes, is about 28×10^{-6}/°C. Therefore, on cooling from the 2600–2900°C test temperature a considerable stress is developed perpendicular to the layer planes on the specimen edges. This stress is relieved by kinking and bending as shown schematically in Fig. 3c (lines represent layer planes; shaded area is carbon deposit). Carbon deposition can be eliminated or greatly reduced by using shields of flexible pyrolytic foil held in close contact with the specimen edge surfaces by carbon yarn ties. When this is done, kink ridge formation is correspondingly eliminated or reduced.

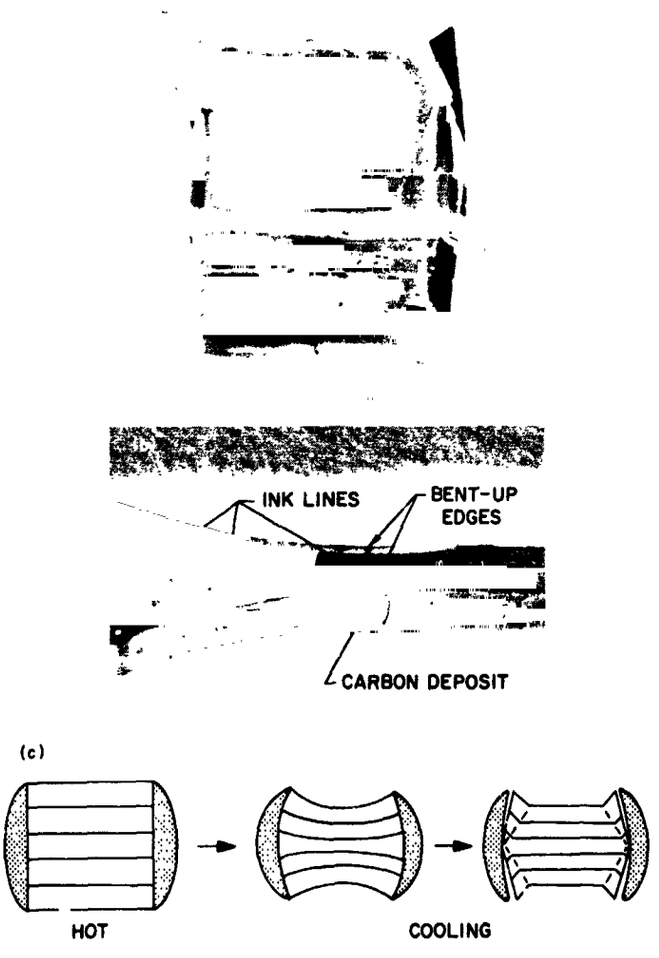

Fig. 3. Bent-up edges on tensile-deformed pyrolytic carbon: (a) transverse cross section of gage region showing bent edges (40×); (b) evaporated carbon deposit on sample sides in throat region and bent-up edges (approximately 4×); (c) schematic of bent edge formation

In specimens tensile-deformed in the as-deposited condition, there is a rather sharp gradient in microstructure and deformation-induced dimension changes in the throat regions at each end of the gage section. In the gage section the material is highly graphitized and very well oriented with very straight layer planes. In the butt and grip portions, the turbostratic, wrinkled sheet structure of the as-deposited carbon is largely retained. Narrow kink bands inclined 45–60 deg to the stress direction are often observed in longitudinal sections (normal to substrate and parallel to stress) of the throat region. An unusually good example is shown in Fig. 4a. More often, a number of short kink bands terminating at the specimen surface or on delamination cracks are seen (Fig. 4b). Kink bands have not been observed in transverse sections of the throat region, or in either transverse or longitudinal sections of the uniform gage region. Evidently, the kinks in the throat help to accommodate the structure and thickness gradient which occurs there. They may

Fig. 4(a). Kink bands in throat region of tensile-deformed pyrolytic carbon; long kink in structure and thickness gradient (40×)

Fig. 4(b). Kink bands in throat region of tensile-deformed pyrolytic carbon; smaller kinks terminating at external or crack surfaces in another specimen (50×)

Fig. 5. Structure at grip interface (at right) of tensile-deformed annealed pyrolytic carbon (40×)

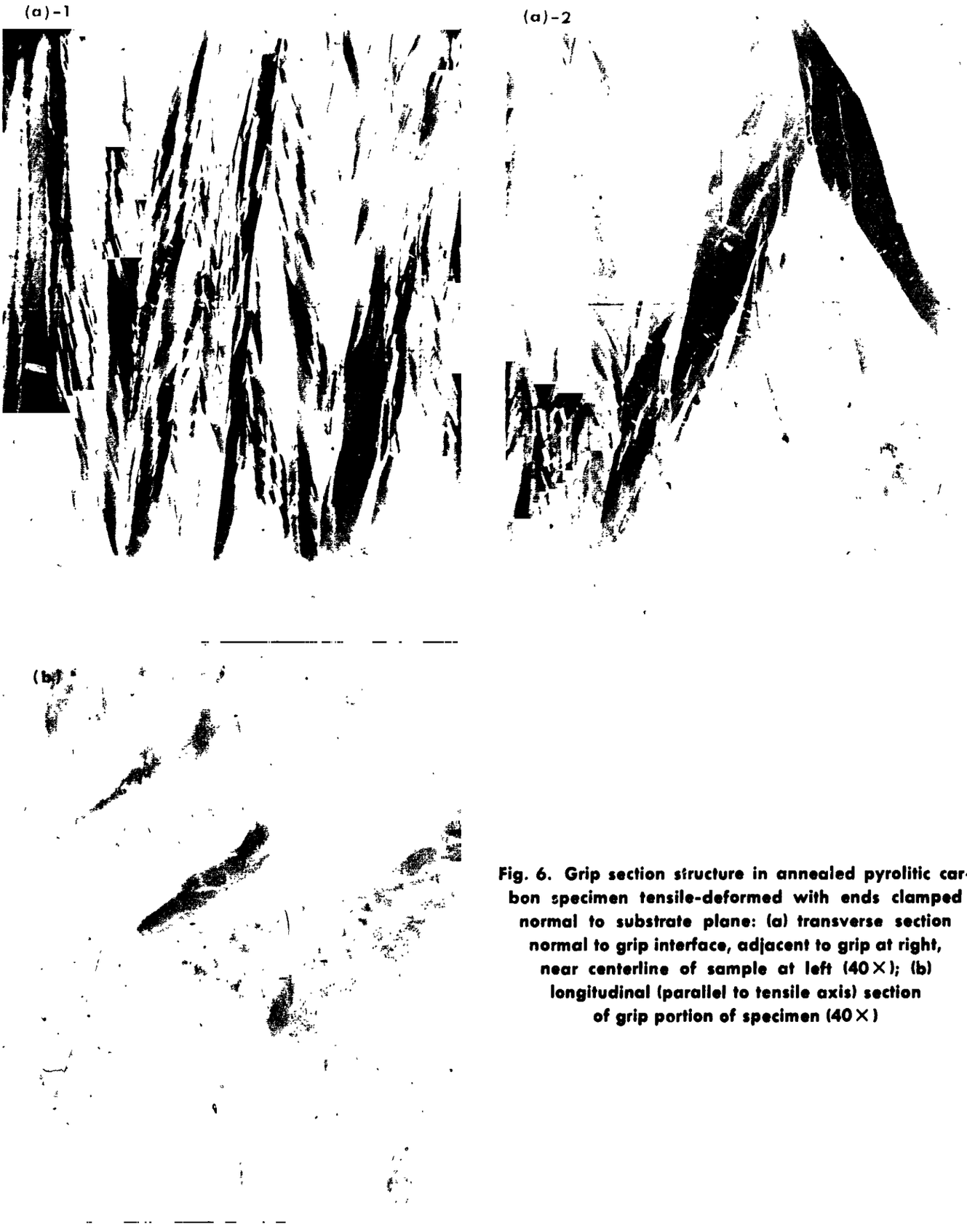

Fig. 6. Grip section structure in annealed pyrolitic carbon specimen tensile-deformed with ends clamped normal to substrate plane: (a) transverse section normal to grip interface, adjacent to grip at right, near centerline of sample at left (40×); (b) longitudinal (parallel to tensile axis) section of grip portion of specimen (40×)

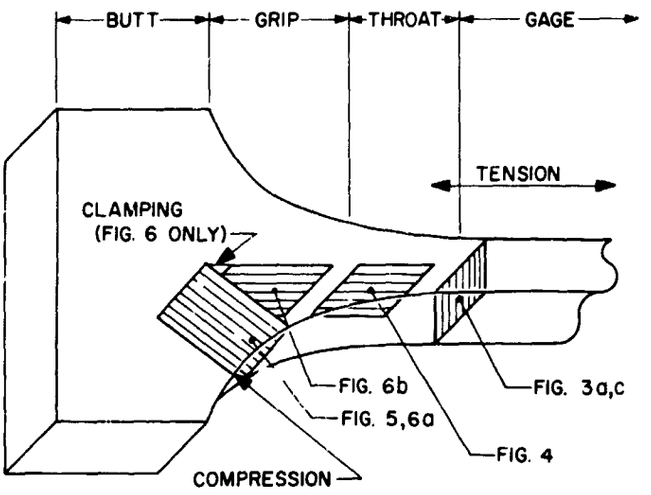

Fig. 7. Location and orientation in specimens of microstructures in Figs. 3–6.

also be associated with bending produced by the slight bow in the substrate "plane" which is characteristic of pyrolytic carbon deposits.

When pyrolytic carbon which has been annealed at 2900°C for 1 hr under 100-psi stress normal to the substrate is tested in tension, most of the recorded elongation results from massive kinking under the compressive stress parallel to the substrate which is developed in the grip region (SPS 37-43, Vol. IV, pp. 121–125). A polarized light micrograph of a cross section of the grip region normal to the radiused grip surface is shown in Fig. 5. Material has been extruded laterally and large diagonal kink bands developed adjacent to the grip surface (at right). However, a short distance from the grip surface the microstructure is the same as in the as-annealed sample (left edge of Fig. 5). If the specimen is tightly clamped laterally (on and perpendicular to the substrate faces), using shims in the grips (SPS 37-43, Vol. IV, pp. 121–125), extrusion is inhibited. A pattern of "flow lines" parallel to the radiused grips on the sample grip region faces shows that deformation effects extend across the whole width of the sample. A cross section normal to the grip surface (Fig. 6a) shows large kink bands near the grip surface (at right) and an unusual chevron-like microstructural pattern which extends to the centerline of the specimen (at left). This latter pattern suggests a polygonized structure with straight orientation-change boundaries approximately perpendicular to the layer planes. There is little delamination cracking. When viewed in a direction approximately normal to the compression direction (longitudinal section) near the center line of the specimen grip region, the microstructure has quite a different appearance, as shown in Fig. 6b. The contrast here evidently results mostly from varying inclination of the layers to the plane of the section. These microstructures resulting from parallel compression of annealed pyrolytic carbon are unusual and do not appear to have been observed before.

These examples illustrate the common occurrence and wide variety of layer-plane kinking and bending in the deformation behavior of graphite. More detailed microstructural investigation will be needed before this type of deformation and its relationship to other deformation mechanisms is fully understood.

B. Pure Oxide Ceramic Research, *M. H. Leipold*

The problem of nonhomogeneous distribution of impurities in ceramic oxides was reported previously (SPS 37-34, Vol. IV, pp. 85–87 and Ref. 2) to be a severe problem and likely to have a significant influence on the behavior of polycrystalline oxides. The previous results did not clarify the mechanism of segregation, and further work has been completed to investigate the driving force for this impurity segregation.

The materials, techniques, and equipment are all identical to those indicated in the reports cited above. The only difference introduced was use of varied specific cooling rates. Two specimens were cut from the same pieces of both Fisher M300 MgO and JPL MgO. They were held in air at a maximum of 2,000°C for ½ hr. The slowly-cooled specimens were cooled at a rate of 50°C/hr to a maximum temperature of 1200°C. At this temperature diffusion rates are too slow to permit additional atomic redistribution in these materials. The quenched specimens were dropped from the furnace chamber at 2,000°C approximately 3 ft into a beaker of distilled water. The cooling rate was such that interior color was no longer visible after approximately 3 sec. Random walk calculations indicate that movement of calcium is less than 0.1 μ for this cooling rate.

Fig. 8 shows the results for calcium (Ref. 3) distribution in relatively large areas (0.16 mm²) of two Fisher M300 MgO specimens that are identical except that they were cooled at different rates. The large amount of segregated calcium in the slow-cooled specimen shows that the movement to the grain boundary occurred primarily upon cooling, although small amounts of segregation did exist in the quenched specimen. Similar results for silicon (not shown) were obtained. Distribution of iron and aluminum was sought but not found. The results for the

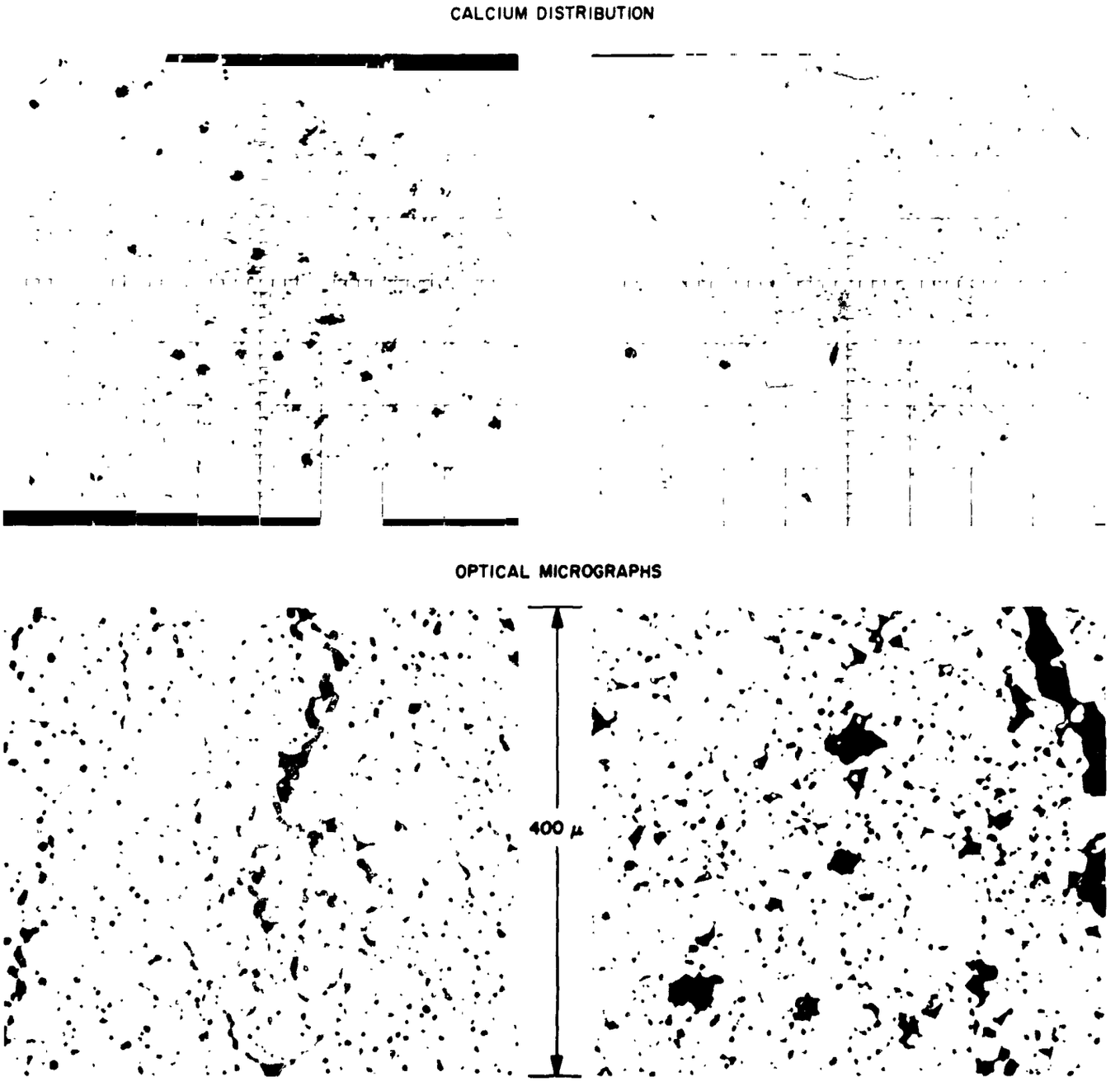

Fig. 8. Calcium distribution in Fisher M300 MgO after heating at 2000°C for ½ hr then cooling

higher purity JPL materials were similar, but were less obvious because of lower total concentration.

Fig. 9 shows calcium and silicon distributions at higher magnification in the slowly-cooled Fisher material. These results are similar to the previously reported work, although less severe because of the lower re-heat temperature (2000 vs 2200°C). Note that the segregated impurities are generally evident as a second phase and largely at triple points.

Fig. 10 shows one of the infrequent segregated regions in the quenched specimen. Note that here the impurities are located along the grain boundaries, and were not optically discernible as second phase. The existence of these impurities in solution in the quenched specimen could be a result of true quenching or merely lower segregated quantities. Consequently, effort was made to find locations having the same concentration of impurity existing as second phase in the slowly-cooled specimens, and in solution in the quenched specimens. This effort was not successful, so true quenching of impurities into solution cannot be claimed.

The difference in behavior between quenched and slow-cooled specimens helps considerably to understand

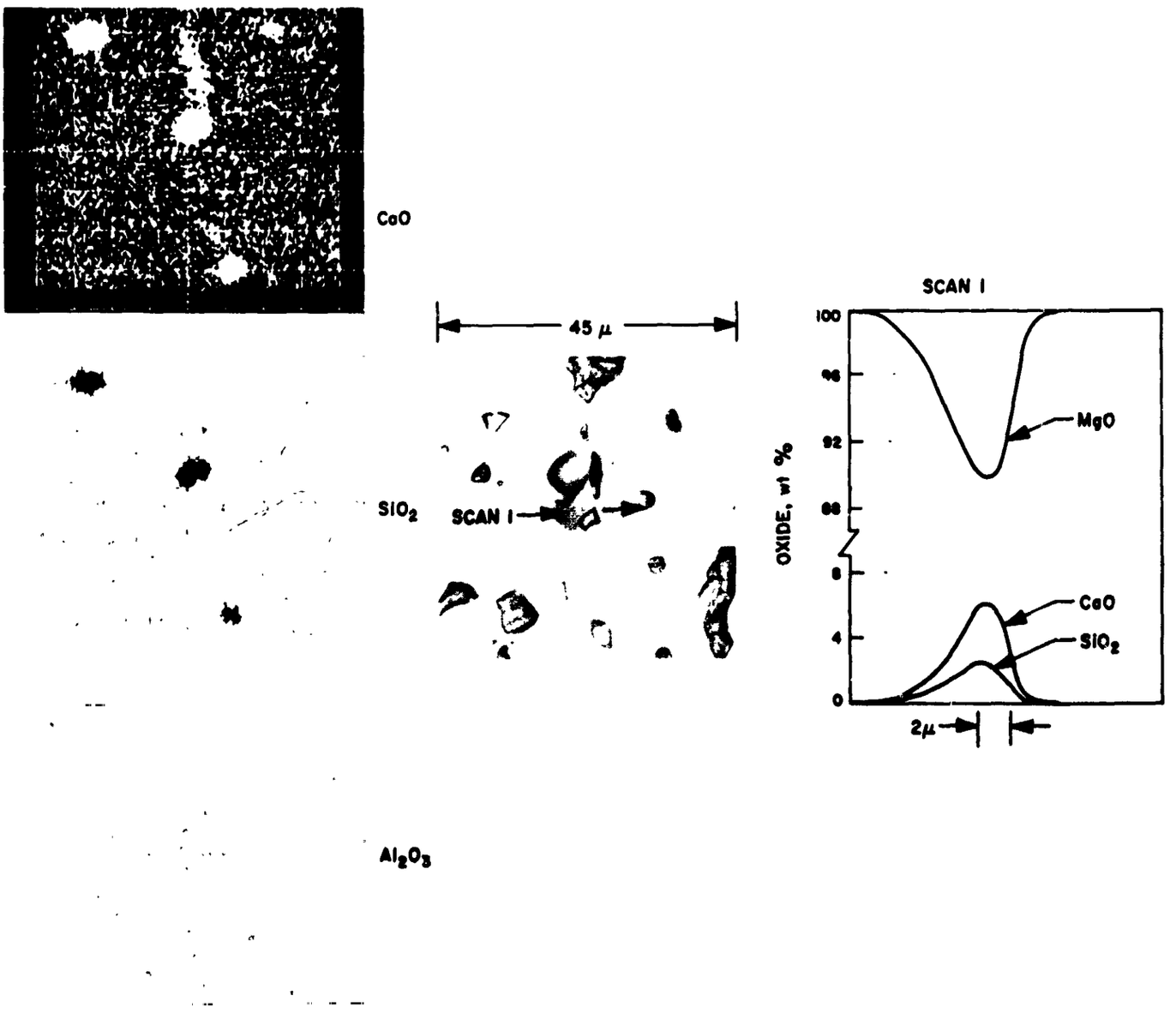

Fig. 9. Impurity distribution in Fisher M300 MgO cooled at 50°C/hr

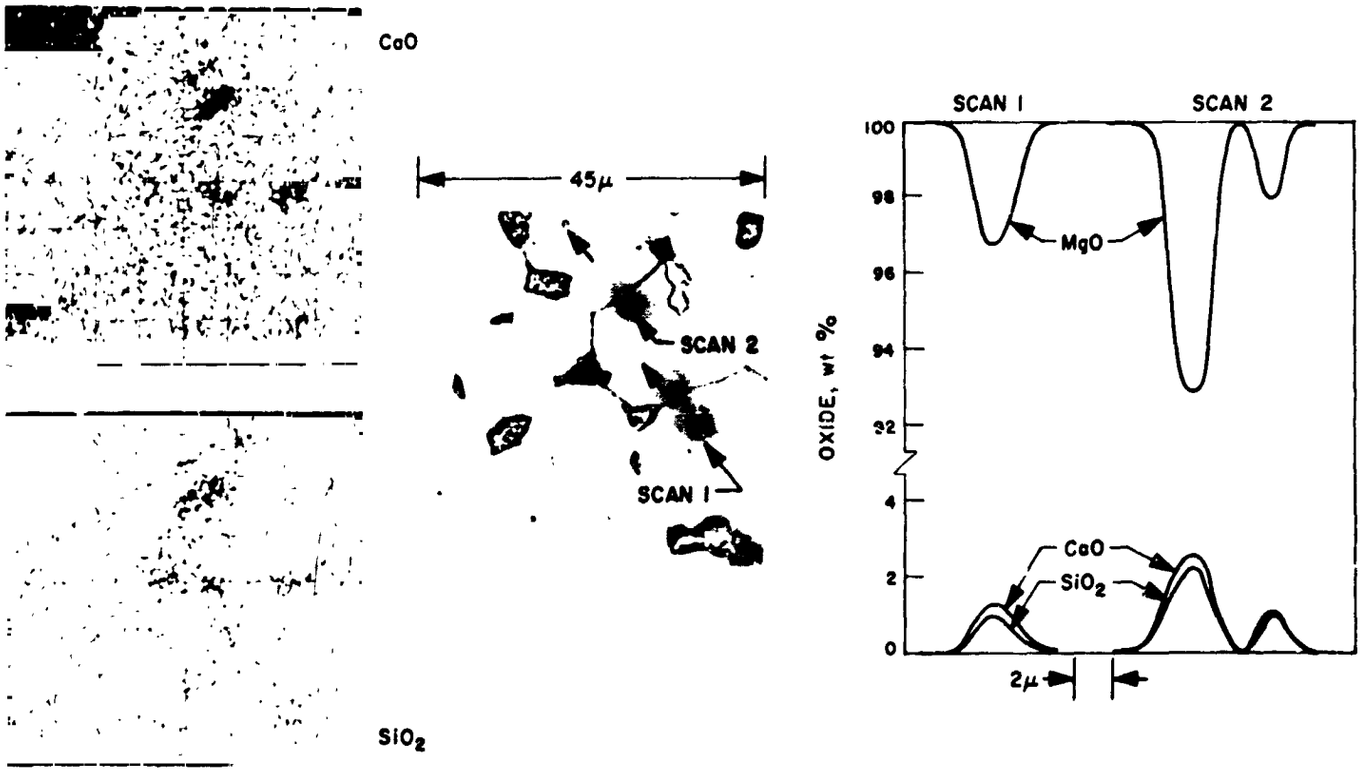

Fig. 10. Impurity distribution in quenched Fisher M300 MgO

the nature of the segregation. The fact that it occurs during the cooling cycle invalidates an equilibrium segregation mechanism as the primary factor. Although differences in energy may still exist for an impurity at a normal lattice site when compared to a grain boundary location, this cannot be the primary factor. Rather, a mechanism of the type proposed by Westbrook[2], et al (Refs. 4 and 5) is supported. They propose that as the number of equilibrium thermal vacancies in the lattice become excessive during cooling, these excess vacancies migrate to the grain boundaries carrying impurities with them. The vacancies are absorbed into the grain boundary leaving the impurity atoms effectively trapped.

C. Heat Shields for Out-of-Orbit Entry into Mars,

R. G. Nagler

Under the auspices of an informal Intercenter *Voyager* Heat Shield Coordination Group with representatives from Ames Research Center, Langley Research Center, and JPL, a preliminary investigation of the available materials for entry into the Martian atmosphere from orbit has been begun. The first phase of this investigation, out-of-orbit ablation screening, is now complete. This phase consisted of a series of 3 test conditions (Table 1) simulating the expected Martian entry environment from out of orbit. The tests were done by Mr. R. Pope of Ames Research Center on materials furnished by JPL.

The test data on these 23 materials are shown in Table 2. The back-surface temperature and the mass of material lost were thought to be sufficient test information for this early screening activity. There were some side

Table 1. Test conditions for out-of-orbit ablation screening activity

Test condition	Cold wall heating rate, Btu/ft² sec	Stream enthalpy, Btu/lb	Pressure, atm	Total heating, Btu/ft²
1	15	1900	0.01	1500
2	30	3500	0.01	1500
3	50	6000	0.01	1500

[2]Westbrook, J. H., "Impurity Effects at Grain Boundaries in Ceramics," *Proceedings of the Third Joint Meeting of the British and Dutch Ceramic Societies*, Bristol, July 1965 (to be published).

Table 2. Preliminary results of ablation screening at Ames Research Center for *Voyager-Mars* out-of-orbit missions

Material	Density ρ, lb/ft^3	Weight ρx, lb/ft^2	Temperature rise at back surface, °K			Total mass loss, %		
			q=15[a]	q=30[a]	q=50[a]	q=15[a]	q=30[a]	q=50[a]
Armstrong cork 2755	31.2	2.0	41	32	31	11.33	12.35	11.72
	31.2	1.0	56	46	37	20.3	22.9	21.4
Armstrong cork 2755 (sterilized)	26.1	2.0	44	36	23	11.39	12.94	12.47
GE 1004AP	33.0	2.0	92	75	64	4.85	5.45	4.80
GE 1004AP (sterilized)	30.5	2.0	89	61	52	3.99	5.0.	4.69
GE 1004AP (low density)	22.2	2.0	57	54	44	3.68	4.77	5.48
	22.2	1.0	137	135	111	4.6	8.6	9.8
Hughes phenolic nylon	36.0	2.0	80	56	42	9.33	10.70	10.93
Avco 5026-39 (with HCG)	33.3	2.0	77	56	49	9.92	10.50	9.84
Avco Mod 5 (purple blend)	42.4	2.0	81	72	62	6.78	7.67	6.67
	42.4	1.0	141	118	103	11.4	15.3	14.3
McDonnell B45 RF (without HC)	40.3	2.0	98	70	62	6.16	7.38	6.23
McDonnell B45 RF (with HC)	37.2	2.0	77	71	63	7.23	7.14	5.84
High density teflon	137.0	2.0	240	176	141	10.65	20.58	18.46
Avco 5026-99	24.3	2.0	51	40	29	8.1	8.3	7.5
	24.3	1.0	86	71	55	13.5	17.6	16.8
Avco foamed teflon	46.8	2.0	68	50	40	22.5	23.9	20.8
Avco foamed teflon	33.7	2.0	49	37	30	25.2	24.8	22.1
Boeing polyborazole	34.9	2.0	52	41	42	11.1	12.3	21.1
Avco 5026-39/p8	33.3	2.0	65	56	48	9.4	9.5	10.0
Avco Mod 7	42.4	2.0	87	69	64	7.6	8.1	7.8
Avco Mod 20	42.4	2.0	75	62	58	8.6	9.1	8.5
McDonnell B 46RF	36.5	2.0	83	64	52	5.9	6.0	6.3
McDonnell B-47RF	25.2	2.0	53	40	35	9.4	12.3	9.4
Avco high cork	23.3	2.0	47	32	28	9.1	10.4	10.0
Lockheed quartz fiber	13.5	1.0	79	58	52	0.6	0.6	1.1
Martin SLA-561	12.5	1.0	62	51	42	11.3	12.0	11.1

[a] q=cold-wall heating rate, Btu/ft^2 sec

heating effects due to the small size of the models (1.25-in. diameter), but these negative effects were similar for all tests and should not affect the relative performance of the various materials significantly.

Several fairly obvious conclusions can perhaps be drawn from Table 2. First, low density is desirable. The lower the density, the lower the thermal conductance, and, therefore, the better the insulation capacity. Second, the use of cork as a filler appears to provide the lowest composite conductance. Cork is the only material available which exists in the form of hollow polygons on the micro level. Third, sterilization is apparently somewhat beneficial since it drives out low-molecular-weight interstitially-absorbed fluids, lessening the composite conductance by more than can be explained by weight loss alone. Fourth, foamed plastics without fillers may be an era with significant future application since foamed teflon, which compares favorably with the more exotic composites, has one of the higher conductances of any pure plastic.

A plot of the temperature rise at the back surface versus density is shown in Fig. 11. For the out-of-orbit

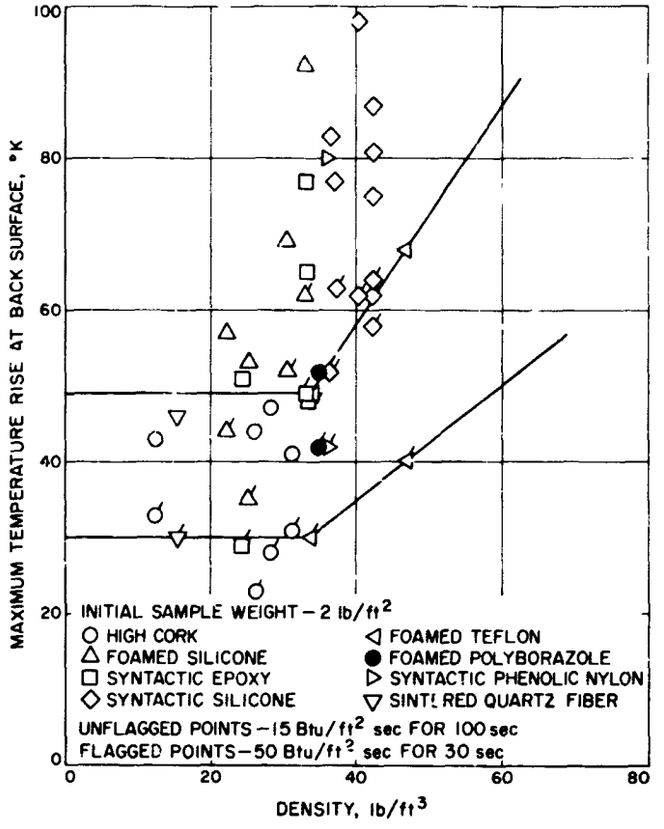

Fig. 11. The effect of density on the insulation capability of various candidate material systems for out-of-orbit entry into Mars

entry use, where the heating loads are small and where the insulation capability is the single most important concept, this figure is somewhat meaningful. The lowest value, regardless of density, represents, of course, the most efficient insulator. On the other hand, if more than one density of the same material is available, the two or more points show a trend which indicates the improvement in insulation capability which might be possible if homogeneous samples could be achieved in even lower densities. Every material has a minimum density into which it may be fabricated in a homogeneous form. This minimum is based on the limitations in the fabrication techniques used to form it into a sample.

An example is shown with the teflon lines drawn on Fig. 11. For its density, foamed teflon appears to be the most efficient material in the figure. The lowest density, though, is presently the lowest available using the given processing method. Hence, the flat extension of the line across the figure to the zero density line results. Any material which is below this line for either heating rate, or which can be hypothesized to be below this line in those lower density versions which could be realistically assumed to be fabricable, is worth investigating further for the out-of-orbit entry mode. Those materials in the figure which meet this criteria are primarily materials high in cork (greater than 50%). A syntactic epoxy foam material, one variety of foamed silicone elastomer, foamed polyborazole, and perhaps the sintered quartz fiber are also somewhat competitive and warrant some further consideration as candidate materials for the out-of-orbit mode of entry into Mars.

Other activities. presently in process, as part of the cooperative efforts of the Intercenter *Voyager* Coordination Group, are sterilization and transit environment screening, an investigation of ablation processes in the direct hyperbolic entry mode into Mars, and the relative RF transparency before and after ablation of the better heat shield materials from the above tests. The results of these activities will be reported as they become available.

References

1. Kotlensky, W. V., "Deformation in Pyrolytic Graphite," *Trans. Met. Soc. AIME*, Vol. 233, pp. 830–832, 1965.

2. Leipold, M. H., "Impurity Distribution in MgO," *Journal of American Ceramic Society*, Vol. 49, No. 9, pp. 498–502, 1966.

3. Rungis, J. and Mortlock, A. J., "The Diffusion of Calcium in Magnesium Oxide," *The Philosophical Magazine*, Vol. 14, No. 130, p. 289, 1966.

References (contd)

4. Aust, K. T., and Westbrook, J. H., "Effect of Quenching on Grain Boundary Hardening in Dilute Pb-Au Alloys," *Lattice Defects in Quenched Metals,* Coltenill, Dayama, Jackson, and Meshii, editors, Academic Press, New York, 1965, p. 771.

5. Seybolt, A. U., Westbrook, J. H., and Turnbull, D., "Mechanism for Grain Boundary and Free Surface Hardening by Oxygen-Vacancy Interactions," *Acta Metallurgica,* Vol. 12, No. 12, pp. 1456–57, 1964.